Study of e^+e^- annihilation to hadrons at low energies at BABAR

V. P. Druzhinin[1,2,⋆]
for the BABAR Collaboration

[1] *Novosibirsk State University, 630090 Novosibirsk, Russia*
[2] *Budker Institute of Nuclear Physics, 630090 Novosibirsk, Russia*

Abstract. New results of study of e^+e^- annihilation to hadrons at low energies at BABAR are presented. The the cross sections for the $\pi^+\pi^-\pi^0\pi^0$, $\pi^+\pi^-\eta$ final states and several exclusive hadronic modes with kaons are measured using the initial-state-radiation technique.

1 Introduction

During the last decade the BABAR experiment [1, 2] at the SLAC National Accelerator Laboratory performs the intensive study of exclusive processes of e^+e^- annihilation into hadrons at low energies using the initial-state radiation (ISR) technique. The main goal of this study is to measure exclusive cross sections for all possible final hadronic states below 2 GeV and calculate the total cross section, which used in Standard Model (SM) calculations of the muon anomalous magnetic moment $a_\mu = (g_\mu - 2)/2$ and the running electromagnetic constant. The different SM contributions to a_μ taken from PDG review [3] are listed in Table 1 together with the experimental result [4]. The leading order (LO) hadronic vacuum polarization contribution ($a_\mu^{\text{had, LO}}$), which is calculated using hadronic cross section data gives a largest contribution into the error of the Standard Model prediction. Currently, about 3.5 sigmas difference is observed between experiment and the SM calculation. New experiments are planned, which will improve accuracy of a_μ measurement by a factor of about 4 [5].

The low energy region, below 2 GeV, give dominant contribution into $a_\mu^{\text{had, LO}}$. The total cross section in this region is calculated as a sum of exclusive channels. Above 2 GeV the total hadronic cross section is measured inclusively. Recently the accurate inclusive measurement was performed in two energy points below 2 GeV (1.84 and 1.94 GeV) in the KEDR experiment [6]. So, the comparison of inclusive and exclusive data and perturbative QCD calculation [7] may be performed in the energy interval between 1.8 and 2.0 GeV. The exclusive data are incomplete near 2 GeV. For example, recently two previously unmeasured processes $e^+e^- \to \omega\pi^0\eta$ and $e^+e^- \to \pi^+\pi^-\pi^0\eta$ were studied in the SND experiment [8, 9], which cross sections are about 5% of the total hadronic cross section near 2 GeV. The BABAR goal is to measure all significant exclusive channels below 2 GeV and perform the comparison with inclusive measurement and pQCD prediction.

Table 1. Contributions to the SM prediction for a_μ (10^{-10}) [3] and comparison with experiment [4].

QED	11658471.895	± 0.008
LO hadronic vacuum polarization	692.3	± 4.2
NLO hadronic vacuum polarization	−9.84	± 0.06
Hadronic light-by-light	10.5	± 2.6
Electroweak	15.36	± 0.10
Theory	11659180.3	± 4.9
Experiment (E821@BNL)	11659209.1	± 5.4 ± 3.3
Experiment − Theory	28.8	± 8.0

In this paper, we will discuss BABAR analyses and preliminary results on the processes $e^+e^- \to \pi^+\pi^-\pi^0\pi^0$, $\pi^+\pi^-\eta$, $K\bar{K}\pi$, $K\bar{K}2\pi$, $K_SK_L\eta$, and $K_SK^+\pi^-\eta$. All measurements are based on data sample with an integrated luminosity of about 470 fb^{-1} collected at center-of-mass energy near 10.6 GeV and use the initial state radiation technique.

2 Initial state radiation method

The mass spectrum of the hadronic system f in the ISR process $e^+e^- \to f\gamma$ is related to the cross section (σ_0) of the nonradiative process $e^+e^- \to f$:

$$\frac{d\sigma(s, m, \theta_\gamma)}{dm\, d\cos\theta_\gamma} = \frac{2m}{s} W(s, x, \theta_\gamma)\sigma_0(m), \qquad (1)$$

where $\sqrt{s}$ is the e^+e^- center-of-mass energy, $x = 2E_\gamma/\sqrt{s} = 1 - m^2/s$, and E_γ and θ_γ is the energy and polar angle of the ISR photon. The function $W(s, x, \theta_\gamma)$ is calculated in QED with a high, better than 0.5%, accuracy.

The ISR photon is emitted predominantly along the e^+e^- collision axis. The produced hadronic system is

⋆e-mail: druzhinin@inp.nsk.su

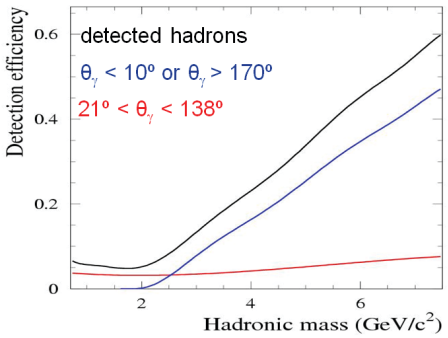

Figure 1. The detection efficiency for $e^+e^- \to 4\pi\gamma$ events obtained using MC simulation as a function of 4π invariant mass. The black curve represents the efficiency with requirement that all final hadrons are detected, the blue and red lines are the efficiencies with additional requirements that the ISR photon is emitted at small and large angles, respectively.

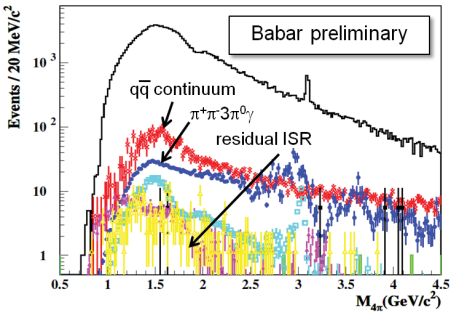

Figure 2. The $\pi^+\pi^-2\pi^0$ mass spectrum for selected data events (black histogram). The mass spectra for background events of different ISR and non-ISR processes calculated using MC simulation are shown by the color histograms.

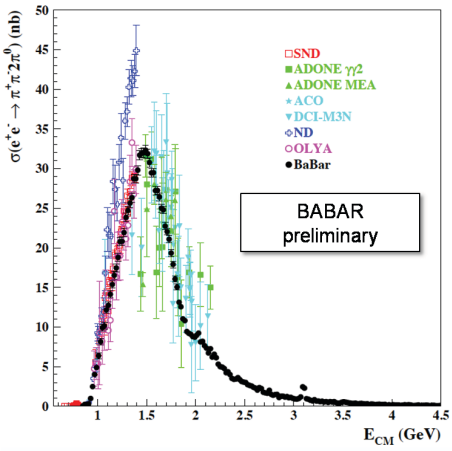

Figure 3. The measured $e^+e^- \to \pi^+\pi^-2\pi^0$ cross section in comparison with previous measurements. The errors are statistical.

boosted against the ISR photon. Figure 1 shows the dependence of the detection efficiency on the hadronic mass for the $e^+e^- \to 4\pi\gamma$ reaction. The black curve represents the efficiency with requirement that all final hadrons are detected. The blue curve is the efficiency with additional requirement that the ISR photon is emitted at small angle, while the red curve is the efficiency with requirement that the ISR photon is emitted at large angle and detected. Due to limited detector acceptance the mass region below 2 GeV can be studied only with detected ISR photon.

The fully exclusive approach is used for low-energy ISR measurements at BABAR. It is required that an event contains a photon with the center-of-mass energy higher 3 GeV and that all final hadrons are detected and identified. Large-angle ISR forces the hadronic system into the detector fiducial volume.

The advantage of the large-angle ISR method over conventional e^+e^- measurements is a weak dependence of the detection efficiency on dynamics of the hadronic system. This allow to measure the total cross section for a multibody final state without detail study of its dynamics with relatively small model uncertainty.

The second advantage is a weak dependence of the efficiency on hadron invariant mass. Measurement in a wide energy range, from threshold up to 4-5 GeV, can be performed with the same selection criteria.

A kinematic fit using requirements of energy and momentum balance improves hadronic mass resolution and provides background suppression.

3 Measurement of the $e^+e^- \to \pi^+\pi^-\pi^0\pi^0$ cross section

The $e^+e^- \to \pi^+\pi^-\pi^0\pi^0$ cross section is one of the least known cross section important for $(g-2)_\mu$.

We select events with all final particles detected and perform the kinematic fit with requirements of energy and momentum balance and two π^0-mass constraints. The requirement on the χ^2 of the kinematic fit ($\chi^2_{4\pi\gamma} < 30$) is applied to select signal events.

The background from the ISR processes with 3 and 5 photons in the final state, $\pi^+\pi^-\pi^0\gamma$, $\pi^+\pi^-\pi^0\eta\gamma$, and $\pi^+\pi^-\eta\eta\gamma$, is additionally suppressed by rejecting events with kinematic fits consistent with those hypotheses; e.g., require $\chi^2_{3\pi\gamma} > 25$. The process with kaons ($K^+K^-\eta\gamma$, $K^+K^-\pi^0\pi^0\gamma$, ...) are suppressed by requiring none of the charged particles to be identified as a kaon.

The largest remaining background is from non-ISR continuum hadronic events, arising from the misidentification of a photon from π^0 decay as an ISR photon. This background is subtracted using MC simulation, which is normalized to reproduce π^0 peak seen in data mass distribution for γ_{ISR} plus any other gamma combinations.

Residual ISR background is subtracted using MC simulation normalized to the existing measurements (rate and shape). The largest ISR background process $e^+e^- \to \pi^+\pi^-3\pi^0\gamma$ is not well measured. The $\pi^+\pi^-3\pi^0\gamma$ mass

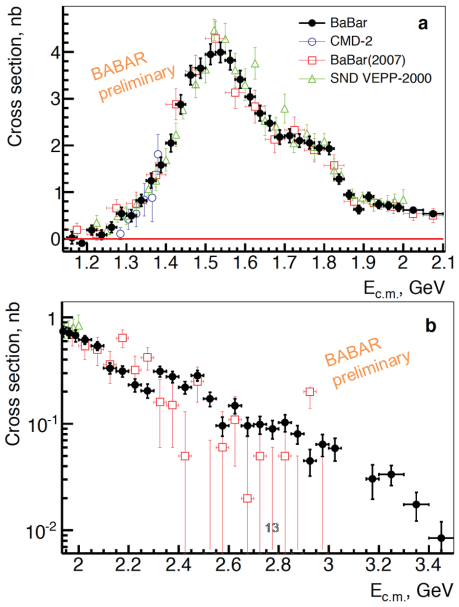

Figure 4. The measured $e^+e^- \to \pi^+\pi^-\eta$ cross section in comparison with previous measurements below 2.1 GeV (a) and between 1.97 and 3.5 GeV (b) on a log scale. The errors are statistical.

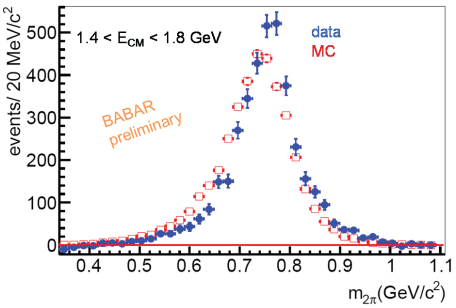

Figure 5. The $\pi^+\pi^-$ mass distribution for selected data events from the $\pi^+\pi^-\eta$ invariant mass range 1.4 – 1.8 GeV in comparison with the same distribution in simulation.

spectrum used to reweight simulation is extracted from BABAR data.

The data $\pi^+\pi^-2\pi^0$ mass spectrum together with the spectra for background events of different ISR and non-ISR processes is shown in Fig. 2. The background is relatively small, about 3% at 1.5 GeV, and about 15% near 4.5 GeV.

The measured $e^+e^- \to \pi^+\pi^-2\pi^0$ cross section in comparison with previous measurements is shown in Fig. 3, The BABAR results are most precise, especially above 1.4 GeV, and covers a wider energy region. The systematic uncertainty of our measurement is 3.1% in the energy region between 1.2 and 2.7 GeV.

The obtained cross section data is used to calculate the contribution from the $e^+e^- \to \pi^+\pi^-2\pi^0$ into $a_\mu^{\text{had, LO}}$. For the energy region below 1.8 GeV it is equal to $(17.9 \pm 0.1_{\text{stat}} \pm 0.6_{\text{syst}}) \times 10^{-10}$. This result can be compared with the previous calculation [10] based on the preliminary BABAR data on $e^+e^- \to \pi^+\pi^-2\pi^0$ from 2007 [11]: $(18.0 \pm 0.1_{\text{stat}} \pm 1.2_{\text{syst}}) \times 10^{-10}$. Our new measurement improves accuracy of this contribution by a factor of 2.

4 Measurement of the $e^+e^- \to \pi^+\pi^-\eta$ cross section

The reaction $e^+e^- \to \pi^+\pi^-\eta$, which is expected to proceed via the $\rho\eta$ intermediate state, is important for spectroscopy of excited ρ-like states.

The process is studied in the $\eta \to \gamma\gamma$ decay mode. Event selection is based on χ^2 of the kinematic fit using requirements of energy and momentum balance. The number of signal events is determined from the fit to the two-photon mass distribution for the η-candidate. The fit removes background from the processes not containing η. Peaked background from ISR ($e^+e^- \to K^+K^-\eta\gamma$, $\pi^+\pi^-\pi^0\eta\gamma$, ...) and non-ISR processes ($e^+e^- \to \pi^+\pi^-\pi^0\eta$, ...) is subtracted using MC simulation normalized as described in the previous section.

The measured $e^+e^- \to \pi^+\pi^-\eta$ cross section is shown in Fig. 4a below 2.1 GeV, and between 1.97 and 3.5 GeV on a log scale in Fig. 4b. The BABAR results in the $\eta \to \gamma\gamma$ decay mode agrees well with the previous measurements, but is more precise and covers wider energy range. The systematic uncertainty near the cross section maximum, 1.35-1.80 GeV, is 4.5%.

Figure 5 represent the $\pi^+\pi^-$ mass distribution for data $\pi^+\pi^-\eta$ events in comparison with the same distribution in simulation. The simulation uses a model with the $\rho(770)\eta$ intermediate state. We confirm the SND observation [12] that the $\rho(770)\eta$ mechanism is dominant, but does not fully describes the $\pi^+\pi^-$ mass distribution observed in data. The observed shift between the data and simulation distributions may be result of the interference with other mechanism, for example, $\rho(1450)\eta$.

The cross section has complex energy dependence. To fit this dependence we use the vector meson dominance (VMD) model with one, two, and three excited states. In Model 1, the cross section data are fitted in the energy range 1.15 – 1.70 GeV with two resonances, $\rho(770)$ and $\rho(1450)$, with the relative phase between their amplitudes equal to π. The fit result is shown in Fig. 6. It is seen that Model 1 cannot reproduce the structure in the cross section near 1.8 GeV. In Models 2 and 3 we include an additional contribution from the $\rho(1700)$ resonance with phases $\phi_{\rho(1700)} = \pi$ and 0, respectively. Both models describe the data below 1.90 GeV reasonably well. There is an additional argument in favor of Model 3: the fitted value of the $\rho(770)$ amplitude better agrees with the its estimation from the $\rho(770) \to \eta\gamma$ decay width. Above 1.90 GeV the fitting curves for both the models lie below the data. Model 4 is Model 3 with a fourth resonance ρ''' added. The fitted energy range is extended up to 2.2 GeV. The fit result is shown in Fig. 6. It is seen that the model suc-

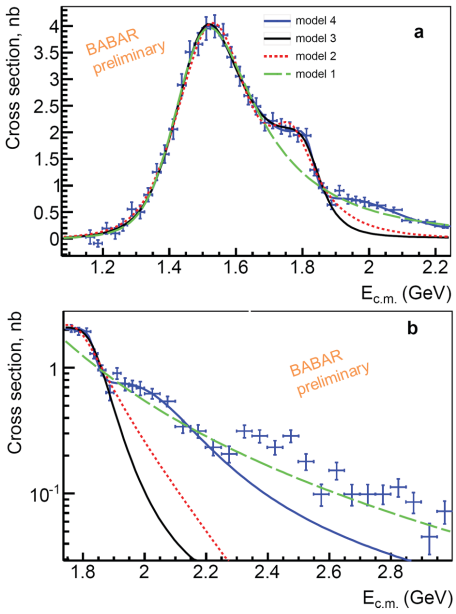

Figure 6. The measured $e^+e^- \to \pi^+ pi^- \eta$ cross section fitted with the four models described in the text.

cessfully describes the cross-section data up to 2.3 GeV. It is interesting that the cross section data from 1.9 to 3.0 GeV is reasonably well described by the simpler model with only one excited resonance.

Under CVC hypothesis, our data on the $\pi^+\pi^-\eta$ cross section can be used to predict the branching fraction for the corresponding τ decay. The CVC prediction based on BABAR data

$$B(\tau^- \to \pi^-\pi^0\eta\nu_\tau) = (0.162 \pm 0.008)\%, \qquad (2)$$

is in good agreement with, but more precise than, the same value based on the SND data [12] $(0.156 \pm 0.011)\%$ and is about 1.8σ higher than the current experimental result for the branching fraction from PDG table [3]. The difference between the CVS prediction and the PDG value, about 15% of the branching fraction, is too large to be explained by isospin-breaking corrections. The PDG value is dominated by the Belle measurement [13] $B(\tau^- \to \pi^-\pi^0\eta\nu_\tau) = (0.135 \pm 0.003 \pm 0.007)\%$ The difference between the CVC-based prediction and Belle result is 2.4σ.

5 Measurement of the $e^+e^- \to K_S K_L \pi^0$ cross section

In this analysis, the K_S is reconstructed via its decay into the $\pi^+\pi^-$ pair. The K_L candidate is identified as an isolated cluster in the electromagnetic calorimeter with the energy deposition larger than 0.2 GeV. The K_L detection efficiency is measured using $e^+e^- \to \phi\gamma$ events, which can be selected without the requirement of detected K_L meson. Figure 7 shows the spectrum of the mass recoiling against the $K_S\gamma$ system in selected $\phi\gamma$ events [14].

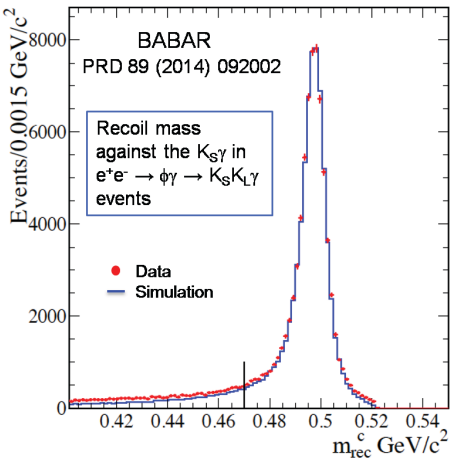

Figure 7. The distribution of the mass recoiling against $K_S\gamma$ system in selected $\phi\gamma$ events in data and simulation.

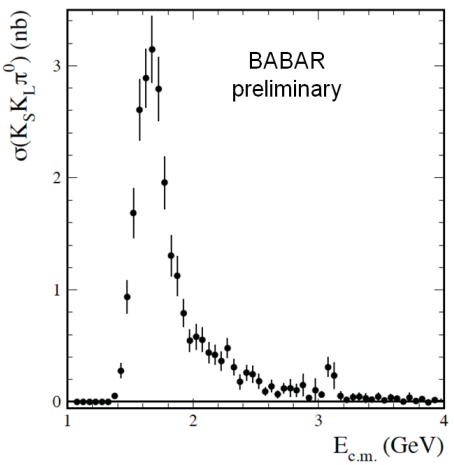

Figure 8. The $e^+e^- \to K_S K_L \pi^0$ cross section measured by BABAR.

Figure 8 represents the first measurement of the $e^+e^- \to K_S K_L \pi^0$ cross section. The systematic uncertainty of this measurement is 10% near the cross-section peak and increases up to 30% at 3.0 GeV.

The dominant intermediate state (more than 95% events) in this reaction is $K^*(892)K$. The $K_2^*(1430)K$ and $\phi\pi^0$ intermediate states are also seen.

Two other charge combinations of the $e^+e^- \to K\bar{K}\pi$ reaction were measured by BABAR previously [15]. So, we can calculate the total $e^+e^- \to K\bar{K}\pi$ cross section without any assumptions about isospin relations between charge modes. The red points in Fig. 9 represent $e^+e^- \to K^+K^-\pi^0$ cross section, the blue points are the sum of the cross sections for $K^+K^-\pi^0$ and $K_S K_L \pi^0$, and the black points are the sum of all three charge modes. The $e^+e^- \to$

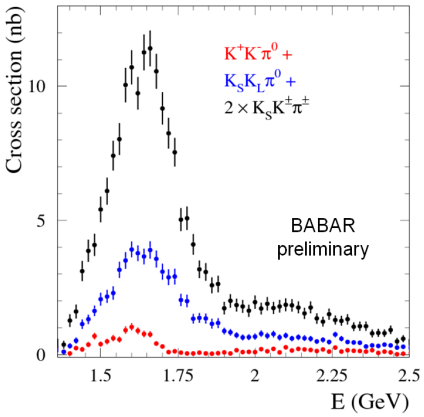

Figure 9. The total $e^+e^- \to K\bar{K}\pi$ cross section obtained as a sum of the cross sections measured in three charge modes: $\sigma(K_SK_L\pi^0) + \sigma(K^+K^-\pi^0) + 2\sigma(K_SK^\pm\pi^\mp)$. The red points represent $K^+K^-\pi^0$ cross section. The blue points are the sum of $K^+K^-\pi^0$ and $K_SK_L\pi^0$ final states.

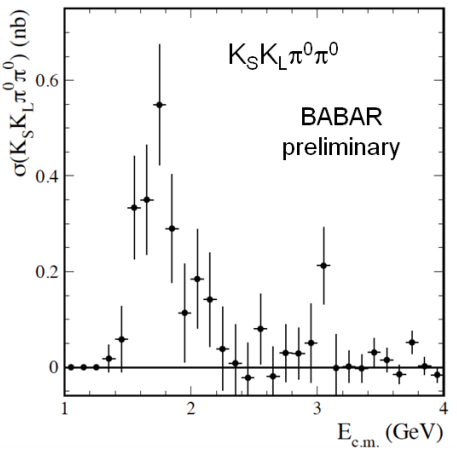

Figure 10. The $e^+e^- \to K_SK_L\pi^0\pi^0$ cross section measured by BABAR.

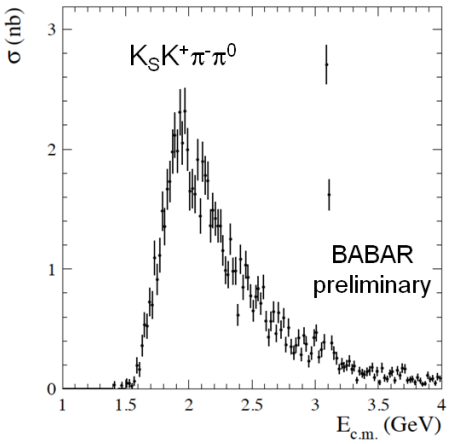

Figure 11. The $e^+e^- \to K_SK^\pm\pi^\mp\pi^0$ cross section measured by BABAR.

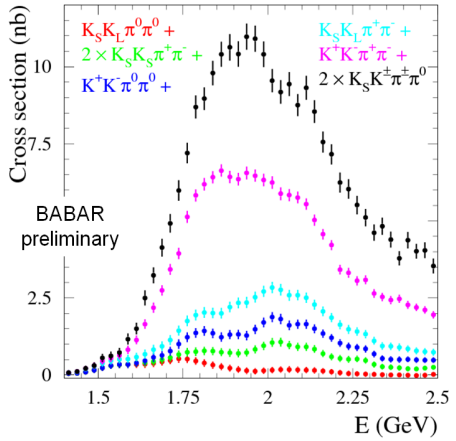

Figure 12. The cross sections for the six charge modes of the $e^+e^- \to K\bar{K}\pi\pi$ process summed cumulatively. The black points represent the total cross section.

$K\bar{K}\pi$ cross section in the maximum is about 12% of the total hadronic cross section.

6 Measurement of the $e^+e^- \to K_SK_L\pi^0\pi^0$ and $e^+e^- \to K_SK^\pm\pi^\mp\pi^0$ cross sections

The process $e^+e^- \to K\bar{K}\pi\pi$ contains six charge combinations. Four of them, $K^+K^-\pi^+\pi^-$, $K^+K^-\pi^0\pi^0$, $K_SK_L\pi^+\pi^-$, and $K_SK_S\pi^+\pi^-$, were measured by BABAR previously [14, 16]. The largest cross section, for $K^+K^-\pi^+\pi^-$ final state, is about 4 nb near 2 GeV.

In Fig. 10 and 11 we present the first measurements of the cross sections for two last charge modes: $K_SK_L\pi^0\pi^0$ and $K_SK^\pm\pi^\mp\pi^0$. Only statistical errors are shown. The $K_SK_L\pi^0\pi^0$ cross section is found to be relatively small and measured with a 25% uncertainty in the peak. The dominant intermediate state for this process is $K^*\bar{K}\pi$. The correlated production of two K^*'s is observed to be small. The $K_SK^+\pi^-\pi^0$ cross section is measured with 6–7% incertainty below 3 GeV. The dominant intermediate states for this reaction are $K^*\bar{K}\pi$ and $K_SK^\pm\rho^\mp$. The correlated $K^*\bar{K}^*$ production is small, less than 15%, and dominated by the charged mode, $K^{*+}\bar{K}^{*-}$.

Now we can calculate the total $e^+e^- \to K\bar{K}\pi\pi$ cross section without any model assumptions. Figure 12 shows the cross sections for the six charge modes summed cumulatively. The black points represent the total cross section. Largest contributions come from the $K^+K^-\pi^+\pi^-$ and $K_SK^+\pi^-\pi^0$ modes. The $e^+e^- \to K\bar{K}\pi\pi$ cross section is about 25% of the total hadronic cross section near 2 GeV.

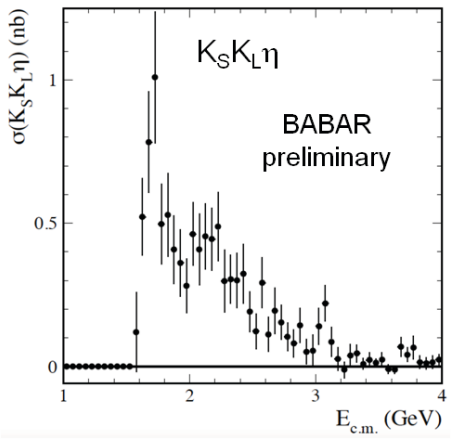

Figure 13. The $e^+e^- \to K_S K_L \pi^0 \eta$ cross section measured by BABAR.

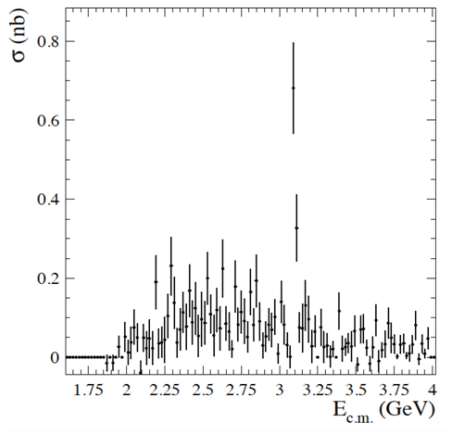

Figure 14. The $e^+e^- \to K_S K^\pm \pi^\mp \eta$ cross section measured by BABAR.

7 The $e^+e^- \to K_S K_L \pi^0 \eta$ and $e^+e^- \to K_S K^\pm \pi^\mp \eta$ reactions

The processes $e^+e^- \to K_S K_L \pi^0 \eta$ and $e^+e^- \to K_S K^\pm \pi^\mp \eta$ are studied for the first time. Their measured cross sections are shown in Figs. 13 and 14.

The $e^+e^- \to K_S K_L \eta$ reaction is dominated by the $\phi\eta$ intermediate state. The cross section agrees with previous BABAR measurements in the $K^+K^-\eta$ mode [15].

The $e^+e^- \to K_S K^\pm \pi^\mp \eta$ reaction is dominated by the $K^*\bar{K}\eta$ intermediate state. The cross section is relatively small and does not contribute to the total hadronic cross section below 2 GeV.

8 Summary

The precise low-energy e^+e^- cross section data are needed to obtain an accurate SM prediction for the muon anomalous magnetic moment. New results from BABAR reduce the respective uncertainty in the contributions from the processes $e^+e^- \to \pi^+\pi^-\pi^0\pi^0$, $\pi^+\pi^-\eta$, $K\bar{K}\pi$, and $K\bar{K}\pi\pi$. Several previously unmeasured processes with kaons, $e^+e^- \to K_S K_L \pi^0$, $K_S K_L \eta$, $K_S K_L \pi^0\pi^0$, $K_S K_L \pi^0\eta$, $K_S K^\pm\pi^\mp\pi^0$, and $K_S K^\pm\pi^\mp\eta$, have been observed and studied. The BABAR ISR program has provided new information about hadronization at low energies and properties of low-mass resonances.

References

[1] B. Aubert *et al.* (BABAR Collaboration), Nucl. Instrum. Meth. A **479**, 1 (2002).
[2] B. Aubert *et al.* (BABAR Collaboration), Nucl. Instrum. Meth. A **729**, 615 (2013).
[3] C. Patrignani *et al.* (Particle Data Group), Chin. Phys. C, 40, 100001 (2016).
[4] G. W. Bennett *et al.* (Muon g-2) Phys. Rev. D **73**, 072003 (2006).
[5] J. Grange *et al.* (Muon g-2 Collaboration), Muon (g-2) Technical Design Report. arXiv:1501.06858 [physics.ins-det].
[6] V. V. Anashin *et al.* (KEDR Collaboration), arXiv:1610.02827 [hep-ex].
[7] P. A. Baikov *et al.*, Phys. Lett. B **714**, 62 (2012).
[8] M. N. Achasov *et al.* (SND Collaboration), Phys. Rev. D **94**, 032010 (2016).
[9] V. P. Druzhinin *et al.* (SND Collaboration), EPJ Web Conf. **130**, 05004 (2016).
[10] M. Davier, A. Hoecker, B. Malaescu and Z. Zhang, Eur. Phys. J. C **71**, 1515 (2011); Erratum: [Eur. Phys. J. C **72**, 1874 (2012)].
[11] V. P. Druzhinin, arXiv:0710.3455 [hep-ex].
[12] V. M. Aulchenko *et al.* (SND Collaboration), Phys. Rev. D **91**, 052013 (2015).
[13] K. Inami *et al.* (Belle Collaboration), Phys. Lett. B **672**, 209 (2009).
[14] J. P. Lees *et al.* (BABAR Collaboration), Phys. Rev. D **89**, 092002 (2014).
[15] B. Aubert *et al.* (BABAR Collaboration), Phys. Rev. D **77**, 092002 (2008).
[16] J. P. Lees *et al.* (BABAR Collaboration), Phys. Rev. D **86**, 012008 (2012).